

Pore Structure Characterization of Porous Films

Christopher L. Glaves,[†] Gregory C. Frye,[†] Douglas M. Smith,^{*,†} C. Jeffrey Brinker,[†]
Abhaya Datye,[†] Antonio J. Ricco,[§] and Stephen J. Martin[§]

UNM Center for Microengineered Ceramics, The University of New Mexico,
Albuquerque, New Mexico 87131, Division 1846, Sandia National Laboratories,
Albuquerque, New Mexico 87185, and Division 1113, Sandia National Laboratories,
Albuquerque, New Mexico 87185

Received October 10, 1988

We have applied two alternative techniques, NMR spin-lattice relaxation of pore fluid and surface acoustic wave (SAW) measurements of adsorbed/condensed gas/vapor, to the analysis of porous materials. These techniques show promise in overcoming the low signal-to-noise problem arising from having a thin porous film on a relatively thick dense or porous substrate, which renders techniques such as mercury porosimetry and nitrogen adsorption/condensation, as they are usually applied with conventional instrumentation, useless. Bulk and thin-film silica xerogels were fabricated with primary particle radius on the order of 10 nm. Three bulk xerogels of varying porosity were studied by using proton NMR relaxation measurements of water at 20 MHz and 303 K. These results were compared with pore size distributions obtained from mercury porosimetry, nitrogen condensation, and high-resolution TEM (HRTEM). In addition, pore size distributions were obtained for porous thin films by using NMR and the desorption branch of SAW measurements of adsorption isotherms for a number of gases and vapors, including N₂ at 77 K. In contrast to the results from the bulk samples, the condensation (SAW-derived) PSD was skewed to larger pore sizes as compared to the NMR-derived PSD. However, this is primarily the result of reduced network/percolation effects associated with the thin film on the SAW device (≈ 5 particles thick) as compared to the bulk samples. The results indicate that both SAW and NMR pore size analysis, which are in good agreement when one considers the different basic phenomena that the two methods probe, can be used to extract meaningful pore size distribution information for porous thin films.

Introduction

Porous films/coatings are used for an increasing number of applications, including protective coatings (i.e., chemical, thermal, etc.), optical coatings, membranes, and catalyst supports. The properties of interest for each specific application are a strong function of the film's pore structure. Pore structure properties of possible interest include total pore volume, porosity, mean pore size, pore shape, pore connectivity, and pore size distribution. The extraction of pore structure information is normally accomplished by using gas adsorption/condensation and/or mercury porosimetry.¹ However, in addition to the normal problems associated with these two methods, the signal-to-noise problem arising from having a thin porous film of low total volume on a relatively thick dense or porous substrate can render these techniques, as they are usually applied with conventional instrumentation, useless.

One solution to this problem is to make a bulk porous material by using the same synthesis scheme as the porous film. Conventional pore structure analysis can be conducted on the bulk sample, and the film's pore structure can be *inferred* from the bulk sample. This approach assumes that a bulk sample can be synthesized via the same process and that the evolution of pore structure during the film and bulk material synthesis is identical. An alternate and more attractive solution to the problem is to explore the use of new pore structure analysis schemes which allow the study of film pore structure directly. Several new pore structure techniques have recently been reported and have promise for obtaining the high signal-to-noise ratios necessary for the characterization of porous films. These include NMR spin-lattice relaxation measurements of fluid in pores¹ and surface acoustic wave (SAW) measurements of organic vapor and nitrogen ad-

sorption isotherms.^{2,3} The potential application of these techniques to the measurement of pore structure in films is the subject of this work.

Background

The basic principle of spin-lattice relaxation measurements for pore structure analysis is that a fluid contained in a porous solid will undergo spin-lattice relaxation at a faster rate than the same fluid under bulk conditions. Initially, this phenomenon was used for qualitative pore size analysis.^{4,5} More recently, this approach has been used to extract pore size distributions for a range of bulk porous materials such as controlled pore glass and sphere packings,¹ coals,⁶ microporous silica xerogels,⁷ and rock.⁸

In order to relate the reduction in the spin-lattice relaxation time, T_1 , to the pore size, the "two-fraction, fast-exchange" model is employed.⁹ Fluid in the pore is assumed to be two distinct phases: a bulk phase, which has the same relaxation properties as bulk fluid, and a surface-affected phase in close proximity to the pore surface for which the relaxation rate is greatly enhanced. If diffusion between the two phases is much faster than the relaxation rate, a single exponential decay will be observed with a characteristic T_1 given by

$$1/T_1 = f_b/T_{1b} + f_s/T_{1\text{surface}} \quad (1)$$

The observed T_1 is a function of the relative fractions of the two phases, f_s and f_b , and the relaxation times for the

(1) Gallegos, D. P.; Munn, K.; Smith, D. M.; Stermer, D. L. *J. Colloid Interface Sci.* 1987, 119, 127.

(2) Martin, S. J.; Frye, G. C.; Ricco, A. J.; Zipperian, T. E. *Proc. 1987 IEEE Ultrasonics Symp.*, IEEE: New York, 1987; p 563.

(3) Ricco, A. J.; Frye, G. C.; Martin, S. J. *Langmuir* 1989, 5, 273.

(4) Brown, R. J. S. *Bull. Am. Phys. Soc.* 1956, 1, 216.

(5) Senturia, S. D.; Robinson, J. D. *Soc. Pet. Eng. J.* 1970, 10, 237.

(6) Glaves, C. L.; Davis, P. J.; Gallegos, D. P.; Smith, D. M. *Energy Fuels* 1988, 2, 662.

(7) Gallegos, D. P.; Smith, D. M.; Brinker, C. J. *J. Colloid Interface Sci.* 1988, 124, 186.

(8) Schmidt, E. J.; Velasco, K. K.; Nur, A. M. *J. Appl. Phys.* 1986, 59, 2788.

(9) Brownstein, K. R.; Tarr, C. E. *J. Magn. Reson.* 1977, 26, 17.

* Author to whom correspondence should be addressed.

[†] UNM Center for Microengineered Ceramics.

[‡] Division 1846, Sandia National Laboratories.

[§] Division 1113, Sandia National Laboratories.

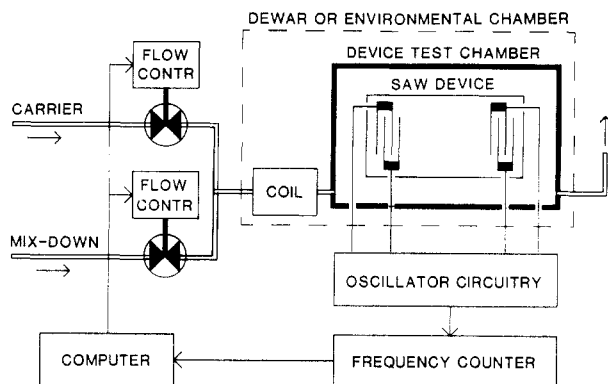


Figure 1. Schematic of a surface acoustic wave device with input and output transducers in the experimental setup for obtaining adsorption isotherms. The fractional saturation pressure (P/P_0) of the adsorbate is varied under computer control by dilution with a nonadsorbing mix-down stream.

two phases. For pores greater than ≈ 5 nm, eq 1 may be rewritten in terms of the pore surface area, SA, to pore volume, PV, ratio:

$$1/T_1 = 1/T_{1b} + (SA/PV)(1/T_{1s}) \quad (2)$$

T_{1s} is not a relaxation time but rather the ratio of the surface phase relaxation time and the thickness of the surface-affected phase. This thickness is usually on the order of one monolayer. If the pore radius, r_p , is defined as the hydraulic radius ($2PV/SA$), an expression relating radius and T_1 is obtained:

$$1/T_1 = \alpha + \beta/r_p \quad (3)$$

where α is $1/T_{1b}$ and is a function of fluid and temperature. The surface interaction parameter β is $2/T_{1s}$ and is a function of temperature, proton frequency, fluid, and surface chemistry. For pores in the size range 0.5–5 nm, a pore shape assumption is required to obtain an expression analogous to eq 3.⁷ In general, the magnitude of β increases with a decrease in proton frequency (field strength).¹⁰ Therefore, for maximum accuracy, this increase in β must be balanced by the corresponding decrease in signal-to-noise ratio associated with decreasing proton frequency. This optimum frequency will be a function of both pore size and the total pore volume in the NMR.

For a porous solid with a distribution of pore sizes, a distribution of T_1 values must be obtained. The T_1 distribution, $f(T_1)$, must be extracted from the magnetization data set, $M(\tau)$, by solving

$$M(\tau) = M_0 \int_{T_{1\min}}^{T_{1\max}} [1 - 2 \exp(-\tau/T_1)] f(T_1) dT_1 \quad (4)$$

where τ is the delay time between the 180° and 90° pulses, M_0 is the equilibrium magnetization, and $T_{1\min}$ and $T_{1\max}$ represent the range of expected T_1 values. For pore size analysis, this has been accomplished by using a nonnegative least-squares approach (discrete distributions)¹¹ and the method of regularization (continuous distributions).^{12,13}

The surface acoustic wave (SAW) device technique is based on the sensitivity of these devices to minute changes in adsorbed mass. This sensitivity has recently been exploited in the construction of a variety of chemical sen-

sors.^{14–19} Detection of mass changes as small as 100 pg/cm^2 has been demonstrated.^{14,15} Figure 1 shows a schematic of the typical configuration of a SAW device. Interdigital transducers at opposite ends of a piezoelectric substrate excite and detect a SAW. When an oscillating electrical potential is applied to the input transducer, an oscillating strain field is created in the piezoelectric substrate, launching the acoustic wave. By use of the output transducer, the acoustic wave, after traversing the length of the crystal, is converted back into an electrical signal. Since nearly all the SAW energy is carried within one acoustic wavelength of the surface, the SAW velocity is sensitive to extremely small changes in surface parameters.²⁰

A simple yet highly accurate method for monitoring acoustic wave velocity is to utilize the SAW device as the feedback element of an oscillator loop (see Figure 1). When the net gain of the loop equals unity, the loop spontaneously oscillates at a frequency for which the round-trip phase shift is a multiple of 2π . Since the separation between input and output transducers is many wavelengths, the majority of the phase shift occurs in the SAW device. Consequently, the SAW propagation velocity (v) controls the oscillation frequency (f). When the SAW velocity is perturbed only by variations in surface mass, frequency changes can be related to the amount of adsorbed mass by

$$\frac{\Delta f}{f_0} = \kappa \frac{\Delta v}{v_0} = -\kappa c_m f_0 m \quad (5)$$

in which κ is the fraction of the SAW path length between transducers covered by the film ($\kappa = 1$ for the thin films examined here), c_m is the mass sensitivity of the device ($1.3 \times 10^{-6} \text{ cm}^2\text{-s}/\text{g}$ for ST quartz),²⁰ v_0 and f_0 are the unperturbed wave velocity and oscillator frequency, respectively, and m is the mass of adsorbed molecules/device area. With our system, frequency stability over short time intervals (1 min) is on the order of 1 Hz or less. Since the devices oscillate at 97 MHz, this represents a resolution of 10 ppb for changes in wave velocity, corresponding to 77 pg/cm^2 of film. This extreme sensitivity to surface mass is the basis for the recently reported use of thin-film-coated SAW devices to measure the mass changes which occur during 77 K N_2 adsorption isotherms.^{2,3,15}

Experimental Section

The silicate sols used for thin-film deposition were prepared by a variation of the Stöber et al.²¹ procedure for synthesizing monodisperse, spherical, silica colloids. Tetraethoxysilane (33.8 mL) was added dropwise to a stirred solution containing 328 mL of absolute ethanol and 10.7 mL of 14.8 M NH_4OH . The solution was stirred for 16 h at room temperature, resulting in a stable sol composed of ~ 20 -nm-diameter, roughly spherical silicate particles. The sol concentration was 3 wt % equivalent oxide (SiO_2).

(14) Martin, S. J.; Ricco, A. J.; Ginley, D. S.; Zipperian, T. E. *IEEE Trans. Ultrasonics, Ferroelectrics and Freq. Contr.* 1987, UFFC-34, p 142.

(15) Frye, G. C.; Ricco, A. J.; Martin, S. J.; Brinker, C. J. *Mater. Res. Soc. Symp. Proc.*; Materials Research Soc.: Pittsburgh, 1988; Vol. 121, p 349.

(16) Martin, S. J.; Schweizer, K. S.; Schwartz, S. S.; Gunshor, R. L. *Proc. 1984 IEEE Ultrasonics Symp.*; IEEE: New York, 1984; p 207.

(17) Chuang, C. T.; White, R. M. *Proc. 1982 IEEE Ultrasonics Symp.*; IEEE: New York, 1982; p 295.

(18) Snow, A.; Wohltjen, H. *Anal. Chem.* 1984, 56, 1411.

(19) Ricco, A. J.; Martin, S. J.; Zipperian, T. E. *Sensors Actuators* 1985, 8, 319.

(20) Auld, B. A. *Acoustic Waves and Fields in Solids*; Wiley: New York, 1973; Vol. 2.

(21) Stober, W.; Fink, A.; Bohn, E. *J. Colloid Interface Sci.* 1968, 26, 62.

(10) Glaves, C. L.; Davis, P. J.; Smith, D. M. *Powder Technol.* 1988, 54, 261.

(11) Munn, K.; Smith, D. M. *J. Colloid Interface Sci.* 1987, 119, 117.

(12) Gallegos, D. P.; Smith, D. M. *J. Colloid Interface Sci.* 1988, 122, 143.

(13) Brown, J. A.; Brown, L. F.; Jackson, J. A.; Milewski, J. V.; Travis, B. J. *Proc. of the SPE/DOE Unconventional Gas Recovery Symp.*, 1982, p 201.

Table I. Physical Properties of the Bulk Silica Xerogels

sample	SA, m ² /g	ϵ^a
STO-225	258	0.51
STO-250-1	340	0.57
STO-250-2	449	0.66

^a Expressed as void fraction.

Thin films were prepared by immersing the substrates (glass microsheet, glass wool, or SAW device) in the sol and withdrawing the substrates at a constant rate by using a computer-controlled dipping apparatus contained in a chamber that maintains a constant relative humidity of <5%. During deposition, the silicate particles are assembled on the substrate surface by a complex process that combines gravitational draining and convective flow due to evaporation of the solvent (ethanol). The microsheet and SAW devices were withdrawn at 8 in./min. In order to minimize detrimental effects of menisci forming between strands of glass wool, the wool was coated at 1 in./min, which results in a reduced film thickness. Despite this precaution, sol menisci formed in some areas, causing thicker film regions that dried more slowly than films deposited on microsheet or SAW substrates.

Following film deposition, all substrates were subjected to a 670 K anneal in air for 5 min. On the basis of ellipsometric measurements, the equivalent thickness and refractive index of the heated films (measured for films deposited under identical conditions on (100) Si substrates) were $t = 150$ nm and $n = 1.24$. With a calculated refractive index of 1.40 for the silicate skeleton, a refractive index of 1.24 corresponds to about 40 vol % porosity.²² The thickness and refractive index values obtained for Si substrates are equivalent to those for films deposited on the flat microsheet and SAW substrates. Wool samples have regions of thinner and thicker films with as yet undetermined refractive indices.

Samples for NMR experiments were saturated with water vapor (film and bulk samples) and aqueous salt solutions (bulk samples). 180°- τ -90° spin-lattice relaxation experiments were performed at 303 K and proton frequencies of 20 and 300 MHz. The low field experiments were performed with a Spin-Lock CPS-2 pulse NMR spectrometer with a magnet field strength of 4.7 kG. The duration of the 90° and 180° pulses was approximately 5 and 10 μ s. The 300-MHz measurements were made with a General Electric GN300 Fourier transform NMR spectrometer with a field strength of ≈ 70 kG. Radio frequency pulse times were 30 and 60 μ s. Typically, the magnetization, $M(\tau)$, was measured at 40 different τ values between 1 ms and 9 s. The T_1 distribution was obtained from $M(\tau)$ by the method of regularization.¹² In order to obtain α and β , T_1 experiments were performed for the two bulk samples at several different water contents, and the water content was determined gravimetrically after each experiment.

In addition to the NMR experiments, nitrogen adsorption/condensation experiments were performed on the three bulk samples to obtain the BET surface area and pore size distribution (desorption branch). Samples were outgassed under vacuum at ≈ 323 K overnight before analysis. Nitrogen uptake measurements were conducted by using an Autosorb-1 volumetric adsorption analyzer. The nitrogen BET surface area and the total porosity, estimated from the nitrogen pore volume, for the three bulk samples are reported in Table I. For two bulk samples, mercury porosimetry measurements were made over the pressure range 12–33 000 psia by using an Autoscan-33 scanning porosimeter. The contact angle was taken to be 140°.

SAW devices were designed at Sandia Labs and fabricated using crystalline ST-cut quartz substrates by Crystal Technologies, Inc. (Palo Alto, CA). Devices have input and output interdigital transducers, each composed of 50 finger pairs formed from 200-nm Au-on-Cr metallization. The periodicity is 32 μ m, and the operating frequency is 97 MHz. Full details of device fabrication have been published elsewhere.^{3,14} After application of the test film, the SAW device is mounted in a 1 \times 0.5 in. flatpack, which is inserted in a brass test case. A Teflon gasket provides a gas-tight seal between the edge of the flatpack and a stainless steel lid

Stober Bulk SA*C Plot: 20 MHz and 300 MHz

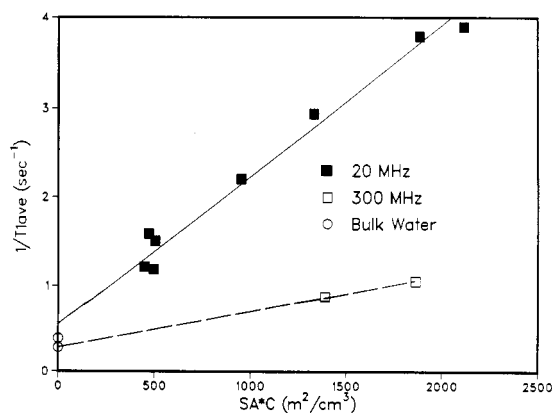


Figure 2. Surface area-concentration plot for determining α and β on bulk silica xerogel.

containing gas inlet and outlet. An oscillator loop is formed by connecting the input and output transducers of the SAW device via a wide-band amplifier; a fraction of the oscillator signal is sent to a frequency counter interfaced with a computer for data acquisition. Additional details of the electronic system are given elsewhere.^{14,19}

After the sample is outgassed for 2 h at ≈ 435 K under dry N₂, the test case containing the SAW device and a stainless steel coil connected to the gas inlet are maintained at the boiling point of the adsorbate by immersion in liquid N₂ or Ar contained in a Dewar flask (Figure 1). By use of mass flow controllers to set flow rates of a N₂ (Ar) stream and a nonadsorbing²³ He mix-down stream, the partial pressure (P) of N₂ or Ar is varied under computer control. For the organic adsorbates, outgassing was done overnight at room temperature under dry N₂. The N₂ carrier stream is saturated by passage through the glass frit of a bubbler containing the organic liquid. The bubbler is immersed in a liquid temperature bath, which is also used to maintain the temperature of an environmental chamber containing the test case and coil. Bath temperature is 298 K. The mass flow controllers are used to set the relative flow rates of the saturated N₂ stream (corrected for the increased flow due to saturation by the vapor) and a dry N₂ mix-down stream to vary the partial pressure of the organic vapor. In all cases, the oscillation frequency is monitored as P/P_0 (P_0 is the saturation vapor pressure of the adsorbate) increases from 0 to around 0.95 and then returns to 0. Obtaining the isotherms over the course of 2 h was found to be sufficient to maintain adsorption equilibrium.³

Transmission electron microscopy was performed on one bulk sample, STO-250-2, and the various film samples by using a JEOL 2000-FX microscope operated at 200 keV. The samples were supported on carbon films mounted on Cu grids. To avoid contamination, the TEM grid was "dipped" into the powder, and no solvents were used at any stage.

Results and Discussion

NMR Calibration. In order to find the parameters α and β , a series of relaxation experiments were performed on two partially saturated bulk samples (STO-225 and STO-250-1). For partially saturated samples, a plot of $1/T_1$ versus SA*C should be linear with slope $\beta/2000$ and intercept equal to α if C is defined as the mass of solid per volume of fluid.¹⁰ By varying the degree of saturation (i.e., changing C), using the nitrogen adsorption-derived surface area, and measuring T_1 , we constructed this type of plot for the two bulk samples. This plot is presented in Figure 2 for proton frequencies of both 20 and 300 MHz. Data points for both samples are included, and no significant difference between the two samples was noted. Least-squares analysis yields α and β of 0.547 s⁻¹ and 3.36 nm/s

(22) Born, M.; Wolf, E. *Principles of Optics*; Pergamon Press: New York, 1975, p 87.

(23) Lowell, S.; Shields, J. E. *Powder Surface Area and Porosity*; Chapman & Hall: New York, 1984.

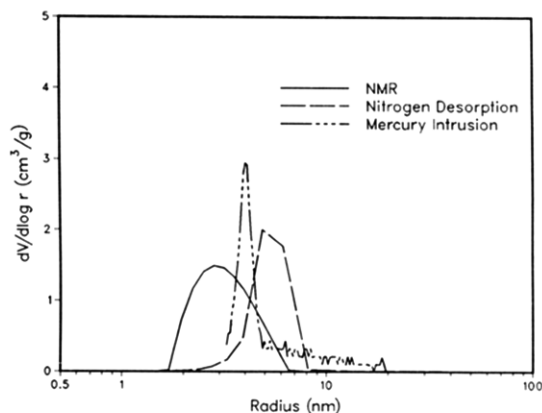


Figure 3. Mercury porosimetry, nitrogen desorption, and NMR pore size distributions for STO-225.

for 20 MHz and 0.277 s^{-1} and 0.949 nm/s for 300 MHz. As with previous studies,^{1,10} surface enhancement of relaxation was found to decrease at higher frequencies.

Comparison of Techniques on Bulk Samples. Pore size distributions have been determined for the bulk samples via NMR and conventional pore sizing methods in order to assess how the pore size distributions (PSD) from the various methods compare. PSDs determined by using the intrusion curve of mercury porosimetry, the desorption branch of nitrogen condensation, and NMR (20 MHz) for the STO-225 sample are given in Figure 3. In principle, mercury intrusion and nitrogen desorption should agree since they employ the same pore shape assumption, and network/percolation effects for intrusion and desorption should be the same. However, the mercury intrusion PSD is shifted to approximately a 30% smaller pore size. Since the pressure-intrusion volume curve is linear, we interpret the apparent intrusion in the size range 5–20 nm to be solely the result of sample compression. This results in a smaller apparent pore size when the pressure of pore filling is reached.

The difference between nitrogen/mercury PSDs and NMR is the result of several factors. In order to relate the applied (or relative) pressure to pore size, a cylindrical pore shape assumption has been made. For NMR, however, a more realistic sphere packing pore model was used. This is not possible for porosimetry/condensation due to the complexities in the calculation of the correct meniscus shape in a sphere packing. Also, the NMR pore size is a hydraulic radius and includes the effect of pore surface roughness (greater roughness implies a smaller pore size will be predicted for the same pore volume). The magnitude of this surface roughness may be estimated by comparing the equivalent diameter of a smooth sphere to the mean primary particle diameter estimated from TEM. Figure 4 is a high-resolution micrograph of the STO-250-2 sample. The micrograph indicates a primary particle diameter on the order 15–20 nm. In contrast, on the basis of the surface area of the sample, the smooth sphere surface area equivalent diameter is 7.3 nm, assuming a density of 2.0 g/cm^3 .

A similar set of PSDs is presented for STO-250-1 in Figure 5. As before, significant sample compression is noted for mercury porosimetry. The 3-nm lower pore size of this plot corresponds to the maximum pressure which could be obtained (33 000 psia). Agreement between the nitrogen desorption and NMR (20 MHz) PSDs is quite good for this sample. As expected for a porous solid formed from a series of primary particles, the distribution of hydraulic radii is broader than the distribution of pore throats (from desorption).¹



Figure 4. HRTEM micrograph of STO-250-2 silica xerogel.

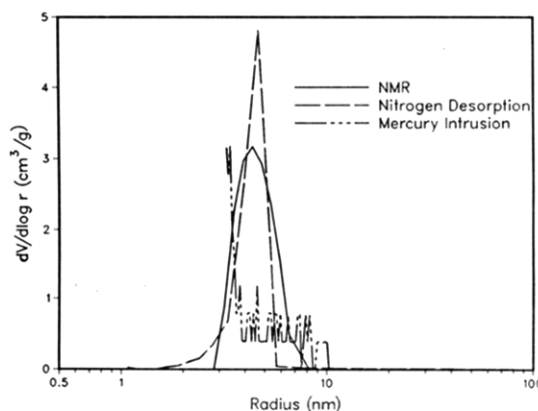


Figure 5. Mercury intrusion, nitrogen desorption, and NMR pore size distributions for STO-250-1.

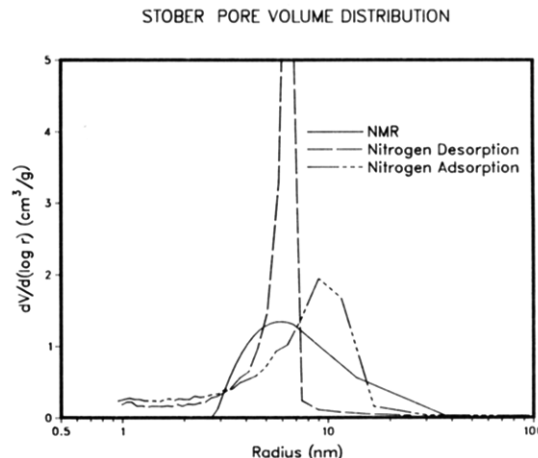


Figure 6. Nitrogen adsorption/desorption and NMR pore size distributions for STO-250-2.

This phenomenon is illustrated more clearly in Figure 6 for the STO-250-2 sample. For this sample, both desorption and adsorption PSDs are presented for comparison to NMR (20 MHz). The adsorption PSD occurs at larger pore size and is broader than the more commonly used desorption branch. The peak width for all three PSDs is broader due to higher porosity, which is the result of different drying history for this xerogel as compared to the two previous samples. In general, excellent agreement between the various pore sizing methods is obtained for the bulk materials when the principles of each technique are considered.

Thin-Film Characterization. For a porous film supported on glass wool, the specific pore volume is sufficient to allow nitrogen condensation to be measured with con-

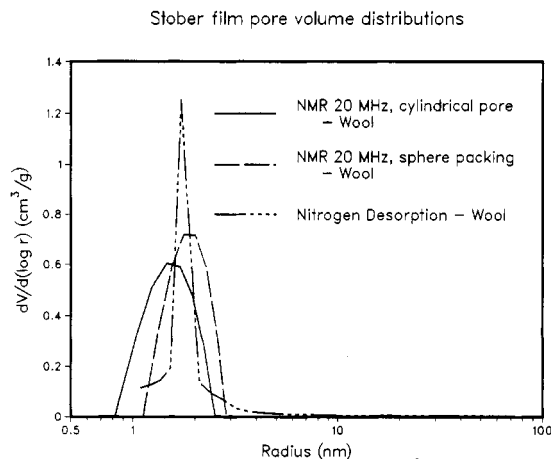


Figure 7. Nitrogen desorption and NMR pore size distributions for silica film on glass wool. NMR pore size distributions are calculated assuming cylindrical- and sphere-packing pore models.

ventional volumetric instruments with some accuracy. PSDs obtained from nitrogen desorption and NMR for this film are presented in Figure 7. For the NMR results, PSDs are presented assuming both cylindrical pores and pores in a packing of uniform solid spheres. Agreement between the two techniques is excellent. However, it should be noted that the pore sizes for these films are significantly smaller than for the bulk samples.

The films tend to have a much smaller porosity, and, for a constant primary particle size, lower porosity results in smaller pore sizes. For a packing of uniform spheres, the average pore size decreases by a factor of 2.25 for a change in porosity from 0.6 to 0.4. Compared to bulk dried gels (xerogels) that are normally formed by slow evaporation of the liquid phase from the gel, dried gel films prepared from solution precursors typically are less porous and contain smaller pores. This trend occurs because gel films are dried in seconds rather than days or weeks typical of bulk, monolithic pieces. For a particular condensation rate, rapid drying greatly reduces the number of condensation reactions that can occur during film formation. Thus, the capillary pressure created by liquid-vapor menisci at the final stages of drying is sufficient to significantly compact the original film structure, resulting in rather dense films with small pores. Slow drying of bulk gels allows many more condensation reactions to occur during drying, strengthening the gel network. The stronger network better resists the capillary pressure, thus reducing the extent of compaction of the structure.²⁴

The argument concerning more rapid drying of films compared to bulk gels could, however, be used to rationalize greater porosity in films than in bulk gels if the sol particles are nonreactive (i.e., if condensation reactions cannot occur). In this case, gel porosity is determined by the extent of rearrangement of the particles (to higher coordination sites) during drying. Rapid drying allows less time for rearrangements to occur, thus potentially resulting in more open structures. However, we suspect that in this case the enormous capillary pressure exerted during the final stages of film drying would tend to efficiently rearrange the particles to a quite dense configuration, regardless of their original packing efficiency.

The pore structure of the glass wool-supported film could possibly be different than the film on a flat solid substrate. Therefore, relaxation measurements were conducted on a film supported on a glass microsheet (80-

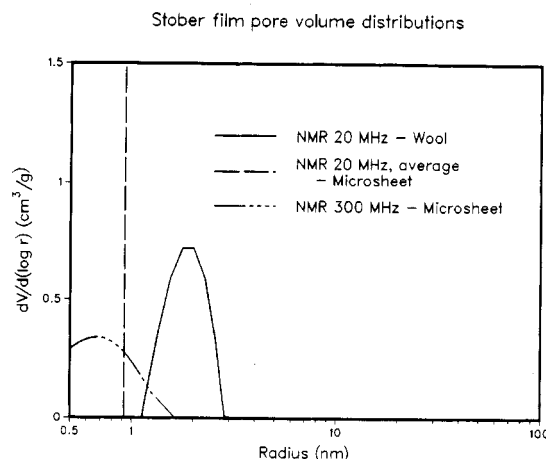


Figure 8. NMR pore size distributions for silica films on glass wool and microsheet.

μm -thick solid substrate with $\approx 0.15\text{-}\mu\text{m}$ -thick porous film on each side). In principle, the pore structure of this film should be quite similar to that contained on the SAW device. From experiments performed at 20 MHz, a distribution of T_1 could not be resolved (because of the low overall porosity of the sample, ≈ 0.001), but the average T_1 indicated a mean pore radius on the order of 0.9 nm. With a higher proton frequency (300 MHz), the signal-to-noise ratio of the NMR measurements was significantly improved, and a T_1 distribution could be resolved. With the 300-MHz α and β values, a PSD was obtained and is presented in Figure 8. The 0.5-nm lower pore size limit corresponds to a pore size for which the "two-fraction fast exchange" can no longer be applied. Also presented in Figure 8 is the 20-MHz NMR PSD for the wool-supported film which was given in Figure 7. A sphere-packing pore model was assumed for all NMR-derived pore size distributions given in Figure 8 and subsequently in the paper since this model most closely resembles the actual pore structure.

The fact that the wool-supported material has a pore size which is much larger than that of the microsheet-supported film is surprising since both materials should have the same primary particle size. The microsheet was expected to have a smaller pore size since it should have a lower porosity; however, the magnitude of the pore size difference and the presence of microporosity were not expected. Therefore, HRTEM was performed on both the glass wool and microsheet-supported films. Micrographs for representative particles of the two films are presented in Figure 9. We should note that TEM sampling was accomplished by scraping film material from the substrate, which explains why the micrographs do not appear as a film. Although the appearance of the glass wool supported film is the same as the bulk xerogel shown previously (Figure 4), the microsheet-supported film is completely different. The microsheet material has a much larger particle size with a different texture. Although the HRTEM micrographs do not provide conclusive proof, it appears, on the basis of both HRTEM and NMR, that these microsheet-supported particles contain microporosity. Therefore, we conclude that the difference in pore size distributions reported in Figure 8 is not the result of the pore size analysis but rather, for some unexplained reason, a physical difference in the two films. Subsequently, HRTEM was performed on all the samples used in this study. All samples had the same appearance except for the microsheet-supported film.

Figure 10 shows examples of adsorption/desorption isotherms for N_2 and Ar obtained by using a coated SAW

(24) Brinker, C. J.; Mukherjee, S. P. *Thin Solid Films* 1981, 77, 141.

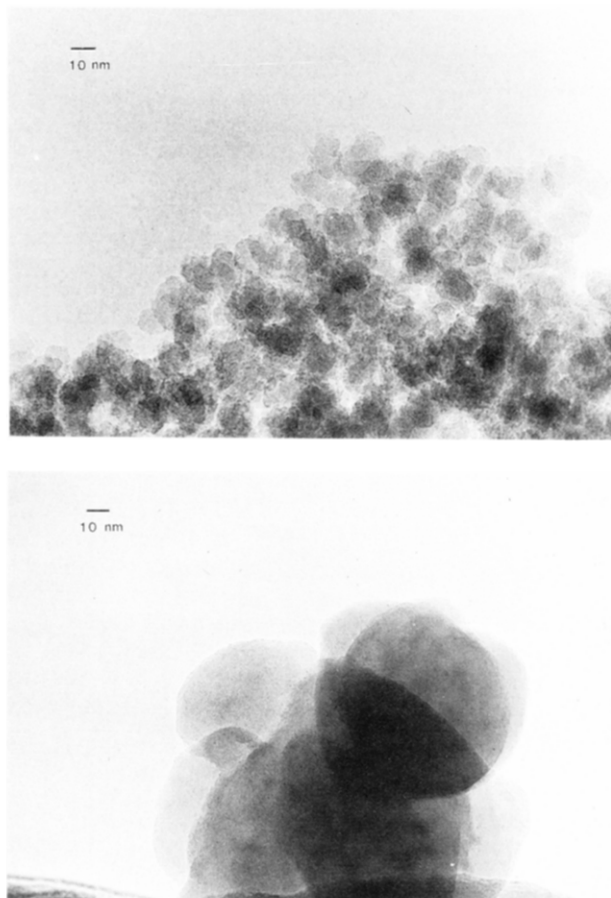


Figure 9. HRTEM micrographs of film on glass wool (top) and microsHEET (bottom).

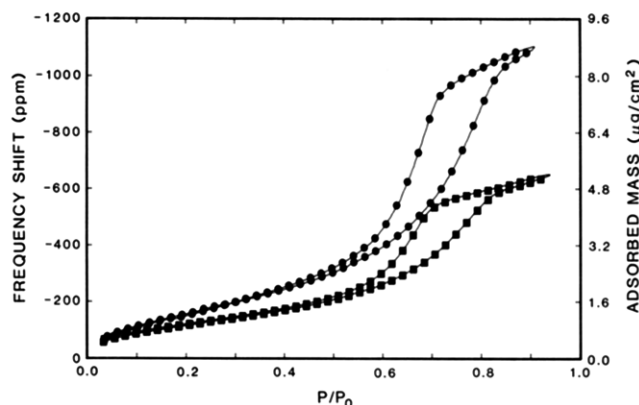


Figure 10. Adsorption/desorption isotherms for Ar (●) and N₂ (■) obtained with coated SAW device 1. The SAW frequency shifts (left axis) are converted to adsorbed mass/area of film (right axis) by using the mass sensitivity constant for the SAW device.

device (device 1). The experimental data are the relative frequency shifts ($\Delta f/f_0$ in ppm) as a function of the relative saturation (P/P_0) in the gas phase over the device. The mass sensitivity constant (c_m in eq 5) is used to convert frequency shift into adsorbed mass per area of film ($\mu\text{g}/\text{cm}^2$). The desorption branch of these isotherms is used to calculate pore size distributions by using standard calculation procedures.²³ The basis for the calculations is 1 cm² of film (rather than 1 g of sample, as is typical for bulk samples). In addition, the surface area of these thin-film samples is low enough that changes in the thickness of the adsorbed layer on the top of the film must be accounted for in the calculation scheme: a starting surface area of 1 cm²/cm² was used for the highest value of P/P_0 .

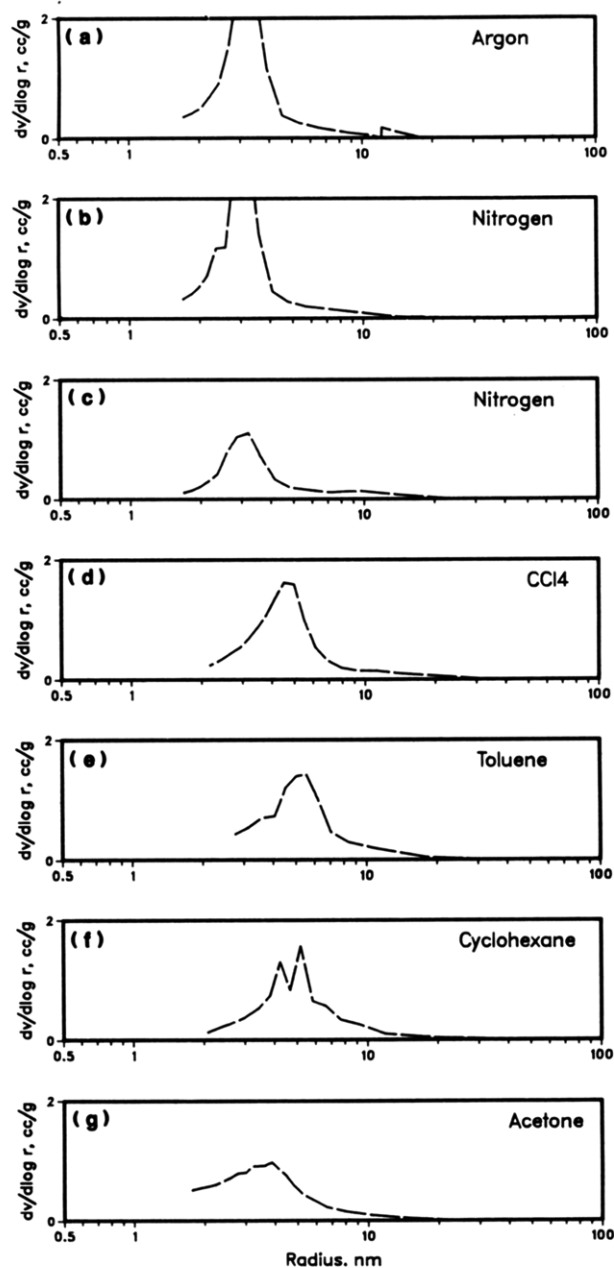


Figure 11. Pore size distributions obtained from SAW device adsorption/desorption isotherms. Calculated values from the desorption branch for device 1 with (a) Ar and (b) N₂ and for device 2 with (c) N₂, (d) CCl₄, (e) toluene, (f) cyclohexane, and (g) acetone.

Figure 11 shows the PSDs calculated from the SAW device data for the various adsorbates. Parts a and b of Figure 11 are based on the data shown in Figure 10 for Ar and N₂ with device 1. The shape of the PSDs is similar as is the median radius (3.4 nm for Ar and 3.2 nm for N₂). Figure 11c shows the results for device 2 with N₂, demonstrating the reproducibility from device to device. Again, the PSDs are very similar, and the median radius (3.4 nm) is close to the values obtained with device 1. Thus, for the standard adsorbates N₂ and Ar, there is good reproducibility between SAW devices as well as consistency between the two species.

The results for organic adsorbates show much more variability in both the shape of the PSD (see Figure 11d-g) and in the median radius (CCl₄, 4.7 nm; toluene, 5.3 nm; cyclohexane, 5.2 nm; acetone, 3.6 nm). Acetone (Figure 11g) has a median radius in line with the N₂ and Ar results, but the shape of the PSD is different. The other three

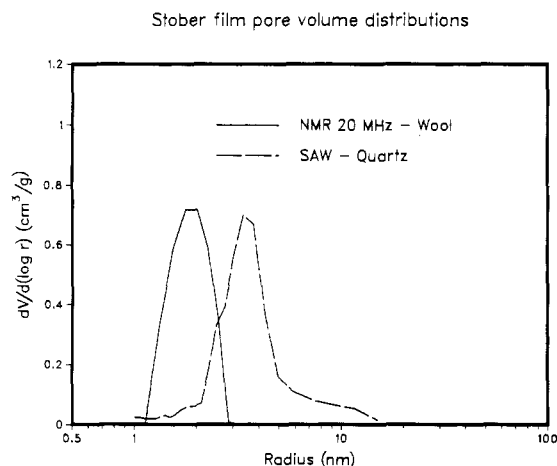


Figure 12. Comparison of NMR pore size distribution for film on glass wool and SAW analysis for film on quartz.

organics are similar in PSD shape to N_2 and Ar, but the median radius is near 5 nm rather than 3 nm. Some possible explanations for these discrepancies are (1) errors in accounting for changes in the adsorbed layer thickness on evacuated pores (the Frankel-Halsey-Hill equation²³ was used for all the adsorbates), (2) effects due to the packing of these larger molecules in the relatively small pores present in the film, (3) differences in the adsorbate surface tension in the small pores,²⁵ or (4) inadequate saturation of the N_2 stream going to the device (calculated P/P_0 values too high, giving larger pore radius). Regardless of the reason, these results are consistent with the observation from bulk samples that probe molecules like N_2 and Ar are the best for obtaining consistent and reproducible results.^{23,25}

Figure 12 shows the SAW/ N_2 desorption and the 20-MHz NMR film on glass wool pore size distributions. Both methods give the same general shape for the PSD. However, the NMR PSD is shifted to significantly smaller pore sizes than the SAW results. For the bulk materials (Figures 3, 5, and 6), NMR and N_2 desorption were in much better agreement even though the two methods should not necessarily agree. In general, NMR, which measures hydraulic radius, should indicate a larger pore size than N_2 desorption, which measures the size of pore constrictions. However, NMR probes surface roughness, and the presence of roughness will result in a smaller pore size. From N_2 /BET surface area and HRTEM measurements, we have shown that the roughness factor (the ratio of BET surface area to geometric surface area) is on the order of 2. Also, this roughness is a function of drying history (note the surface area differences reported in Table I). N_2 desorption pore size analysis is affected by a number of considerations, including assuming that the pores are cylindrical in order to apply the Kelvin equation, assuming that all pores are directly connected to the surface instead of through a complex network of various pore sizes (so-called network/percolation effects), and correctly accounting for the presence of the adsorbed film on the pore wall. Since NMR and N_2 desorption were in close agreement for the film on glass wool sample (which had a thicker film than the SAW device or microsheet), we conclude that the differences between the NMR and SAW results in Figure 12 are not because of any shortcoming with either technique but rather because of a result of differences in the magnitude of network/percolation effects

(25) Gregg, S. J.; Sing, K. S. W. *Adsorption, Surface Area and Porosity*; Academic Press: New York, 1982.

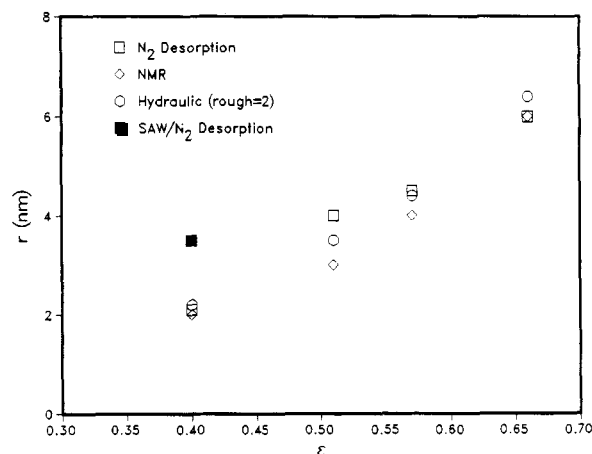


Figure 13. Mean pore radius (r) from nitrogen desorption, NMR, and hydraulic radius (assumed roughness = 2) as a function of porosity (ϵ).

for N_2 desorption between bulk samples and the thin film on the SAW device. The film on the SAW device is only ≈ 5 particles thick, and one would certainly expect network effects to be less important than for a bulk material with the same porosity and primary particle size. The result of increased network effects for desorption is to skew the pore size distribution to smaller pore radii. For example, Iczkowski²⁶ has modeled mercury intrusion for random sphere packings (essentially the same network problem as N_2 desorption) using a percolation model. In that work, a significant surface effect was demonstrated that, for a film with thickness equal to five particles, would indicate a pore size 15–20% larger than for the corresponding bulk material.

Since the pore size distributions for different samples varied significantly, we have explored the effect of porosity (ϵ) on pore size. In particular, the maximum in the PSD as a function of porosity is presented in Figure 13 for both NMR and N_2 desorption. Also included in Figure 13 is the calculated mean hydraulic radius, $2\epsilon r_s/[3(1-\epsilon)]$, for which we have assumed that the particle radius, r_s , is 10 nm and the roughness factor 2. The film porosity is assumed to be 0.4. As expected, the mean radius decreases with decreasing porosity for all three pore size measures. The porosity variation of NMR and hydraulic radius is almost identical, as might be expected since NMR is a measure of the distribution of hydraulic radii. Also, the variation of the N_2 radius with porosity closely follows the NMR and hydraulic radius for the bulk and film on glass wool samples. From the approximate mensicus curvature calculations for sphere packings conducted by Mayer and Stowe,²⁷ one would expect the variation in N_2 radius to approximately track the hydraulic radius. The fact that the mean pore size obtained from analysis of N_2 desorption data for the SAW device is larger is further evidence that network/percolation effects are skewing the bulk N_2 results to smaller pore size.

Conclusions

By use of both NMR spin-lattice relaxation measurements and SAW measurements of gas/vapor adsorption/condensation, pore size analysis of porous thin films has been demonstrated. The two methods are in reasonable agreement when one considers that the two methods are probing different measures of pore size (i.e., hydraulic radius for NMR, pore constriction size for SAW/conden-

(26) Iczkowski, R. P. *Ind. Eng. Chem. Fundam.* 1967, 6, 256.

(27) Mayer, R. P.; Stowe, R. A. *J. Colloid Interface Sci.* 1965, 20, 893.

sation). For a given thin-film pore size application, each of the two methods has particular advantages and disadvantages. The SAW approach has a higher sensitivity (i.e., can be used with thin films with very low porosity) and is based upon a generally accepted technique (gas/vapor condensation). Disadvantages include those normally associated with condensation pore sizing (network/percolation effects, pore shape assumptions, limited pore size) as well as the experimental difficulties associated with making the SAW measurements (i.e., no commercial instruments are available). NMR has advantages such as no pore shape assumption, fast analysis time, a much wider range of sample configurations (i.e., does not need to be deposited on a planar substrate) and no network effects. It is also easier to implement experimentally. The major disadvantage is the lower sensitivity as compared to SAW analysis.

Acknowledgment. The work performed at the University of New Mexico has been funded by Sandia National Laboratories under contract 55-6778. The work performed at Sandia National Laboratories was supported by the U.S. Department of Energy under contract DE-AC04-76DP00789. P. Davis of UNM performed some of the 20-MHz NMR measurements, and C. Gasparovic of the

UNM Center for Non-Invasive Diagnosis performed the 300-MHz experiments. C. S. Ashley of Sandia prepared the film and bulk samples used in this study as well as performed the ellipsometer analysis.

Nomenclature

C	mass of solid/volume of fluid (g/cm^3)
c_m	mass sensitivity of SAW device ($\text{cm}^2\cdot\text{s}/\text{g}$)
f_0	unperturbed SAW oscillator frequency (s^{-1})
f_b	fraction of pore fluid with bulk properties
f_s	fraction of pore fluid in surface-affected phase
$M(\tau)$	magnetization at time τ
M_0	equilibrium magnetization
m	adsorbate mass/area (g/cm^2)
P	adsorbate partial pressure (Torr)
P_0	adsorbate saturation pressure (Torr)
PV	pore volume (cm^3/g)
r	mean pore radius (nm)
r_p	hydraulic pore radius, $2\text{PV}/\text{SA}$ (nm)
r_s	particle size (nm)
SA	surface area (m^2/g)
T_1	spin-lattice relaxation time (s)
T_{1b}	T_1 of bulk phase (s)
$T_{1\text{min}}$	minimum expected T_1 (s)
$T_{1\text{max}}$	maximum expected T_1 (s)
$T_{1\text{surface}}$	T_1 of surface-affected phase (s)

Adsorption of Pyrazine at the Polycrystalline Gold-Solution Interface

Anna Iannelli, Jocelyn Richer, and Jacek Lipkowski*

Guelph-Waterloo Center for Graduate Work in Chemistry, Guelph Campus, Department of Chemistry and Biochemistry, University of Guelph, Guelph, Ontario, Canada N1G 2W1

Received July 20, 1988. In Final Form: December 16, 1988

The thermodynamics of pyrazine adsorption onto a polycrystalline gold electrode was investigated quantitatively by employing chronocoulometry. The measurement of the charge density on the metal side of the metal-solution interface allowed the determination of the adsorption parameters. The film and surface pressures, the relative Gibbs surface excesses, the free energies of adsorption, and the electroadsorption valency as functions of both electrode potential and surface charge density were calculated. The maximum Gibbs surface excess found for pyrazine is $5.8 \times 10^{-10} \text{ mol cm}^{-2}$. The Gibbs free energy of adsorption determined at the potential and charge of maximum adsorption (0.25 V (SCE) and $17.5 \mu\text{C cm}^{-2}$, respectively) is equal to $-32.8 \text{ kJ mol}^{-1}$. The adsorption of pyrazine on Au and Hg is compared, and the differences in the orientation of pyrazine molecules at the two interfaces are also discussed. In addition, the similarities between the adsorption of pyrazine and pyridine on a polycrystalline gold electrode are described.

Introduction

This work is part of a project devoted to studying the influence of the crystallographic orientation of gold electrodes on the adsorption of neutral organic molecules from aqueous electrolyte solutions. The adsorption of pyrazine on a gold polycrystalline electrode is described in this paper.

Pyrazine is particularly well suited to probe the molecular properties of the metal-solution interface. The pyrazine molecule is symmetric and rigid, so it is easy to determine its orientation at the metal surface. The isolated molecule has no permanent dipole moment. Therefore Conway et al.¹⁻³ have suggested that the adsorption of

pyrazine at the mercury-solution interface does not contribute to the surface potential. In consequence, the changes in potential drop across the interface, caused by the replacement of a solvent monolayer by a monolayer of pyrazine, can be taken as a measure of the surface potential generated by the preferentially oriented solvent molecules.

Pyrazine is structurally related to pyridine, which has a large permanent dipole moment. Comparison of pyrazine and pyridine adsorption can therefore be useful to assess the effect of the permanent dipole moment on molecular orientation at the metal-solution interface. The adsorption of pyridine has been recently investigated in our laboratory.^{4,5} Thus the present study constitutes a valuable

(1) Conway, B. E.; Dhar, H. P. *Croat. Chem. Acta* 1973, 45, 109.

(2) Conway, B. E.; Dhar, H. P.; Gottesfeld, S. *Colloid Interface Sci.* 1973, 43, 303.

(3) Conway, B. E.; Angerstein-Kozłowska, H.; Dhar, H. P. *Electrochim. Acta* 1974, 19, 455.